RSC Advances

PAPER

View Article Online
View Journal | View Issue

Cite this: *RSC Adv.*, 2016, **6**, 106866

Nanoarchitectures of self-assembled poly(styrene-*b*-4-vinyl pyridine) diblock copolymer blended with polypeptide for effective adsorption of mercury(II) ions†

Yi-Syuan Lu,[ab] Bishnu Prasad Bastakoti,[b] Malay Pramanik,[b] Md. Shahriar A. Hossain,[c] Saad M. Alshehri,[d] Yusuke Yamauchi*[bcd] and Shiao-Wei Kuo*[a]

Received 20th September 2016
Accepted 18th October 2016

DOI: 10.1039/c6ra23431c

www.rsc.org/advances

We blended the diblock copolymer poly(styrene-*b*-4-vinyl pyridine) (PS-*b*-P4VP) with polypeptides. The pyridyl rings of the P4VP block segment interacted through intermolecular hydrogen bonds with the phenolic hydroxyl groups on the side chains of poly(tyrosine) (PTyr), thereby enhancing the glass transition temperatures (T_g) as a result of their miscibility and changed morphology. The addition of hexamethylenetetramine (HMTA) then led to crosslinking of the phenolic hydroxyl groups of PTyr. The crosslinked PS-*b*-P4VP/PTyr materials displayed superior thermal properties. Because mercury ions tend to bind to the pyridyl rings of P4VP and the amido groups of PTyr through ionic dipole interactions, these materials adsorbed mercury with very high efficiency.

Introduction

The rise in environmental awareness has led to commitments to minimize the environmental impact of heavy metals. Biopolymers are particularly applicable for this because of their environmental friendliness, biocompatibility and biodegradability,[1–6] and rich structural diversity.[7] The well-defined secondary structures, namely, the α-helix and β-sheet structures of polypeptides, which can form intra- and inter-molecular hydrogen bonds,[8,9] enable them to blend with other block copolymers[10–14] and make them useful for adsorbing toxic metals.[15,16] For example, the miscibility of blends of poly(γ-methyl L-glutamate) (PMLG), poly(γ-ethyl L-glutamate) (PELG), and poly(γ-benzyl L-glutamate) (PBLG) with phenolic resin or polyvinylphenol (PVPh) is influenced dramatically by intermolecular hydrogen bonding of the side chains of the polypeptides.[11] In another study, PBLG was blended with polystyrene (PS), poly(acetoxystyrene) (PAS), and PVPh. The different strengths of the resulting noncovalent interactions (π–π, dipole–dipole, and hydrogen bonding, respectively), affected the secondary structures formed by PBLG.[12] In addition to polyglutamates, poly(tyrosine) (PTyr) (a hydrogen bond donor through the phenolic hydroxyl groups on its side chains) also can form a miscible blend with poly(4-vinyl pyridine) (P4VP) (a hydrogen bond acceptor), stabilized through intermolecular hydrogen bonding; the resulting secondary structures can also be controlled by varying the polarity of the solvent.[13] Furthermore, a miscible rod–rod polypeptide blending system, PTyr/PMLG, has been prepared, taking advantage of the hydrogen bonding interactions between the phenolic hydroxyl groups of PTyr and the side-chain C=O groups of PMLG.[14]

The self-assembled structures formed from polypeptide-based copolymers in solution have also been widely examined. For instance, poly(ethylene glycol)-*b*-poly(L-lactide)-*b*-poly(L-glutamic acid) (PEG-*b*-PLLA-*b*-PLGA) has been synthesized as a novel biodegradable ABC-type triblock copolymer.[17] It can be made to self-assemble into spherical micelles by varying the volume ratio of water to *N*,*N*-dimethylformamide (DMF) and pH. Raula *et al.* created polypeptide-based aerosol nanoparticles by ionically complexing poly(L-lysine) (PLL) with the surfactant dodecylbenzenesulfonic acid (DBSA) in various solvents.[18] In these systems, however, the polypeptides formed stable micelle-shaped structures, but they self-assembled only in the liquid phase with no morphological change.

Here, we have developed a block copolymer/polypeptide blend system, using poly(styrene-*b*-4-vinyl pyridine) (PS-*b*-P4VP) and PTyr. PS-*b*-P4VP is widely used block copolymer in self-assembled macromolecular systems, particularly because they can self-assemble into a variety of nanostructures,

[a]*Department of Materials and Optoelectronic Science, Center for Nanoscience and Nanotechnology, National Sun Yat-Sen University, Kaohsiung 80424, Taiwan. E-mail: kuosw@faculty.nsysu.edu.tw*

[b]*International Center for Materials Nanoarchitectonics (MANA), National Institute for Materials Science (NIMS), 1-1 Namiki, Tsukuba, Ibaraki 305-0044, Japan. E-mail: yamauchi.yusuke@nims.go.jp*

[c]*Australian Institute for Innovative Materials (AIIM), University of Wollongong, Squires Way, North Wollongong, NSW 2500, Australia*

[d]*Department of Chemistry, College of Science, King Saud University, Riyadh 11451, Saudi Arabia*

† Electronic supplementary information (ESI) available: Details of curve fitting about secondary structure based on FTIR analyses, XRD, DSC, TGA of PS-*b*-P4VP/PTyr before and after curing with HMTA. See DOI: 10.1039/c6ra23431c

including lamellae, cylinders, and spheres.[19–25] The degree of microphase separation can be affected by varying the types of functional groups and the blend ratio. Due to sharp contrast in polarity between the two blocks of PS-*b*-P4VP, it has been extensively studied to form polymeric blends, although, to the best of our knowledge, the use of polypeptides to initiate phase transitions in the bulk state has not been reported as yet. Furthermore, the self-assembled structure of PS-*b*-P4VP blended with PTyr shows remarkable performance towards the adsorption of Hg(II) ions (Scheme 1).

Mercury (Hg) is a cumulative poison, mainly damaging the human central nervous system and kidneys even at very low concentrations.[26–28] Many studies have focused on mercury removal using polymer blends; for example, poly(vinyl alcohol)/poly(ethyleneimine) (PVA/PEI) and PVA/P4VP by the Lebrun-Corporation.[29,30] Those studies have revealed that the efficiency of P4VP is higher than that of PEI because protonated P4VP tends to bind mercury ions more strongly. In an alternative approach, Chen *et al.* employed an extracellular biopolymer, poly(γ-glutamic acid) (γ-PGA), to adsorb mercury by binding with both its carboxylate and amido groups.[16] In this present study, we added hexamethylenetetramine (HMTA) to crosslink the PTyr segments and, thereby, enhance the mechanical and thermal properties of the PS-*b*-P4VP/PTyr blend system, stabilizing the material against disorder in aqueous solution. The crosslinked PS-*b*-P4VP/PTyr has both attractive structural properties and excellent mercury adsorption capability, potentially leading to higher-efficiency wastewater quality indicators.

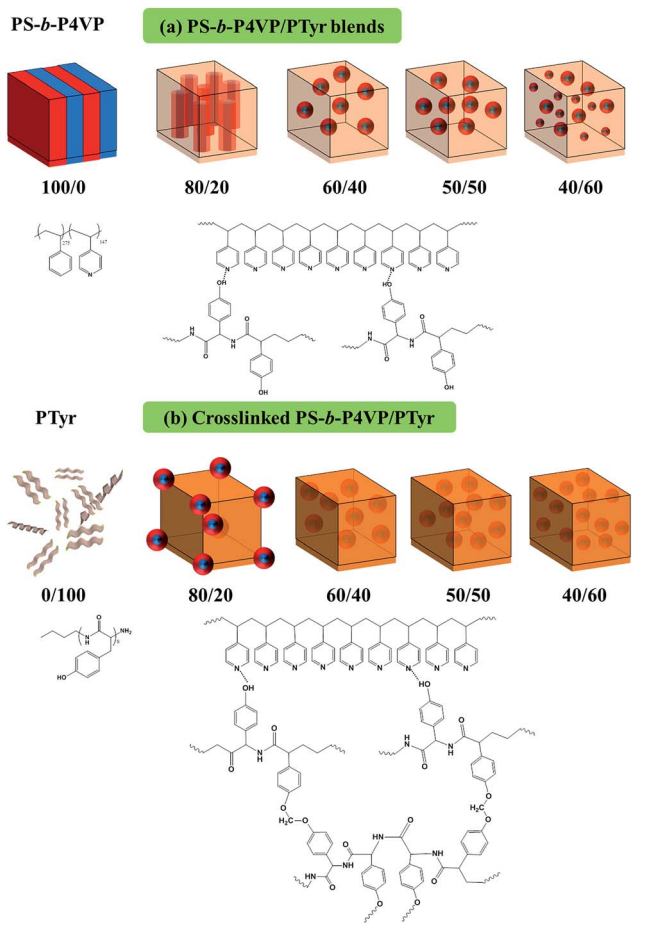

Scheme 1 Self-assembled structures of (a) PS-*b*-P4VP/PTyr blends. (b) Crosslinked PS-*b*-P4VP/PTyr blends.

Experimental section

Materials

The PS_{275}-*b*-$P4VP_{147}$ diblock copolymer was synthesized through sequential anionic polymerization [M_n = 42 000 g mol^{-1}; polydispersity index (PDI) = 1.02]. PTyr [M_n = 1300 g mol^{-1}; PDI = 1.08] was prepared through ring-opening-polymerization (ROP) of L-tyrosine *N*-carboxyanhydride monomer.[13] DMF (Echo, 99.5%) was dried and distilled prior to use. Hexamethylenetetramine (HMTA), mercury(II) nitrate, and acetic acid (0.1 M, pH = 2.85) were used without purification.

PS-*b*-P4VP/PTyr blends and crosslinking reaction

PS-*b*-P4VP and PTyr were dissolved in various weight ratios in DMF (5 wt%). HMTA was added to each blend at a content that was twice the molar amount of the phenolic hydroxyl groups of PTyr. After stirring for 6 h at room temperature, the mixtures were dried in a vacuum oven at 60 °C for two days. The crosslinking reaction was performed by heating sequentially a 100 °C for 2 h, 150 °C for 1 h, and 190 °C for 0.5 h.

Mercury adsorption

A crosslinked blend system (2 mg) was immersed in Hg(II) solution (340 mg L^{-1}, 10 mL, pH 2.85). The solution was collected by filtering after stirring for 24 h at room temperature, and the concentration of Hg(II) was determined by inductively coupled plasma-optical emission spectrometry (ICP-OES).

Characterization

Differential scanning calorimetry (DSC, Hitachi HT-Seiko Instrument SII Exster X-DSC7000) was performed to determine the glass transition temperature (T_g); heating and cooling were performed from −90 to +250 °C under N_2 at the rate of 20 °C min^{-1}. The specific interactions between functional groups were observed using Fourier transform infrared (FT-IR) spectroscopy with a Thermoscientific Nicolet 4700 spectrometer operated at a resolution of 4 cm^{-1}; the samples were prepared in KBr. Thermogravimetric analysis/differential thermal analysis (TGA/DTA, Hitachi HT-Seiko Instrument Exter 6300 TG/DTA) was performed to determine the thermal stability, over a temperature range from 30 °C to 800 °C under air atmosphere. Crystal structures were determined through wide-angle powder X-ray diffraction (XRD, Rigaku RINT 2500X, CuKα radiation, 40 kV, 40 mA) at a scanning rate of 0.5 min^{-1}. Small-angle X-ray scattering (SAXS) was performed at the BL17A1 wiggler beamline of the National Synchrotron Radiation Research Center (NSRRC), Taiwan (diameter and wavelength of X-ray beam: 0.5 mm and 1.1273 Å, respectively; Q range: 0.015–0.3 Å^{-1}). Transmission electron microscopy (TEM, JEOL 2100 microscope) images were collected at 200 kV after

staining with I_2 (P4VP domains). The adsorption of mercury was determined using ICP-OES (720 ES, Agilent, Santa Clara); a gold solution was added to the sample solutions to minimize the memory effect from mercury on the ICP-OES instrument.

Results and discussion

Fig. 1a displays the DSC analysis of the PS-*b*-P4VP/PTyr blend systems with different weight ratios. The pure PS-*b*-P4VP diblock copolymer displayed two glass transition temperatures, at 103 °C and 151 °C for the PS and the P4VP block segments, respectively. The pure PTyr had a value of T_g of 162 °C. The DSC traces recorded after blending the block copolymer with the PTyr homopolymer retained the two glass transition temperatures, implying the microphase separation. The glass transition temperature representing the PS block segment remained nearly the same, 100 °C, but an obvious increase in the value of T_g by 20–30 °C compared to the pure P4VP and the PTyr analogue was observed after forming the P4VP/PTyr complex, presumably because of strong intermolecular hydrogen bonding between the pyridyl rings of P4VP and the phenolic hydroxyl groups of PTyr. This positive deviation from the linear rule (dashed line) was fitted by the Kwei equation (solid line) as displayed in Fig. 1b and described by eqn (1):[31]

$$T_g = \frac{W_1 T_{g1} + k W_2 T_{g2}}{W_1 + k W_2} + q W_1 W_2 \quad (1)$$

where W_1 and W_2 represent the weight fractions of P4VP and PTyr, respectively; T_{g1} and T_{g2} are the glass transition temperatures of pure P4VP and PTyr, respectively; k and q are fitting constants. The strength of the interactions in a blend system is particularly evident in the value of the parameter q. After fitting with the Kwei equation (solid line), we obtained values for k and q of 1 and 135, respectively (Fig. 1b). In a previous study, we also obtained a value of $k = 1$, but values of $q = 100$ and 135 in blended and complexed systems, respectively (by choosing solvents of different polarities, *i.e.*, methanol and DMF, respectively).[13] In this present study, however, P4VP still

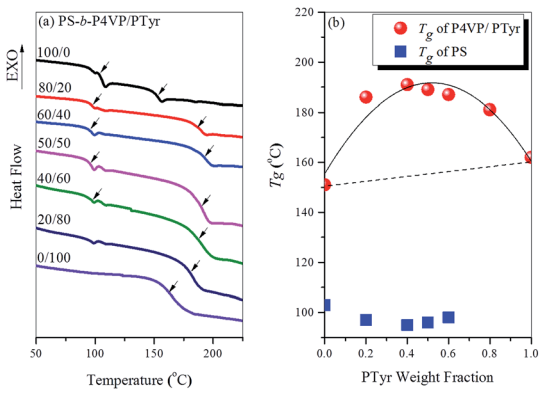

Fig. 1 (a) DSC traces of PS-*b*-P4VP/PTyr blends with various ratios of PS-*b*-P4VP to PTyr; second heating runs for determination of the values of T_g. (b) Glass transition behavior based on the Kwei equation (with the solid line and the dashed line showing by the linear rule and the Kwei equation, respectively, $k = 1$, $q = 135$).

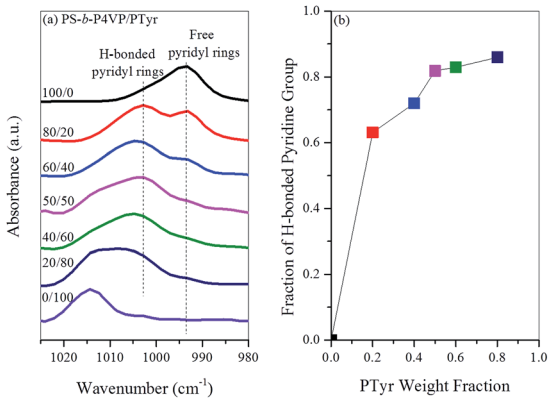

Fig. 2 (a) FT-IR spectra displaying signals for the pyridyl functional groups in PS-*b*-P4VP/PTyr in different weight ratios. (b) Fraction of pyridyl groups of P4VP hydrogen-bonded to the polypeptide, plotted with respect to the PTyr content in the blend systems.

complexed with PTyr, even though we had used a high-polarity solvent (DMF), presumably because of nano-confinement of the diblock copolymer segments as a result of the microphase separation. PTyr prefers to interact with P4VP blocks rather than with PS blocks. As a result, the chain mobility of the P4VP/PTyr complex phase was restricted because of the ordered nanostructure and more compact packing. This phenomenon resulted in a relatively smaller free volume with a higher glass transition temperature. Ultimately, the interactions between P4VP and PTyr were strengthened and the value of q was high, even though the blend was in a high-polarity solvent.

FT-IR spectra can reveal details of the specific interactions in polymer blend systems. Fig. 2a presents FT-IR spectra collected in the wavenumber range from 1025 to 980 cm^{-1}. The spectrum of pure PS-*b*-P4VP featured a characteristic band at 993 cm^{-1}, corresponding to free pyridyl rings, and there was a signal at 1013 cm^{-1} from pure PTyr. After blending PS-*b*-P4VP with PTyr in various weight ratios, the intensity of the band for the free pyridyl rings decreased, and a new band appeared near 1003 cm^{-1}, which was assigned to the hydrogen-bonded pyridyl rings in this blend system. These three peaks could be resolved well by Gaussian functions, as displayed also in Fig. 2a and S1 in the ESI.† The fraction of hydrogen-bonded pyridyl units of P4VP at 1003 cm^{-1} increased with increasing concentration of PTyr. Fig. 2b and Table 1 summarize the results.

The XRD patterns indicated that the secondary structure of PTyr changed after blending with the PS-*b*-P4VP diblock copolymer (Fig. S2a†). The XRD peaks at 18° and 20° confirm the β-sheet secondary structure of pure PTyr. These indicate the distance between the polymer chains of each antiparallel β-pleated sheet and the repeated residues of the chain, respectively.[13] On blending with PS-*b*-P4VP diblock copolymer, the pattern turned into an amorphous halo. Similar behavior was also observed in the FT-IR spectra in Fig. S2b.† We observed eight major peaks for pure PTyr: for ring vibrations at 1597 and 1615 cm^{-1}; for the β-sheet conformation at 1630 cm^{-1}; for the α-helical conformation at 1655 cm^{-1}; for the β-turn conformation at 1670 cm^{-1}; and for the random coil conformation at 1643,

Table 1 Fractions of hydrogen-bonded units in PS-*b*-P4VP/PTyr blends

	Free pyridyl rings			H-bonded pyridyl rings		
PS-*b*-P4VP/PTyr	ν (cm^{-1})	$W_{1/2}$ (cm^{-1})	A_f (%)	ν (cm^{-1})	$W_{1/2}$ (cm^{-1})	A_b (%)
80/20	993	9	36.9	1003	12	63.1
60/40	994	9	28.0	1004	13	72.0
50/50	994	8	18.1	1004	14	81.9
40/60	994	8	17.0	1004	12	83.0
20/80	994	8	14.0	1004	10	86.0

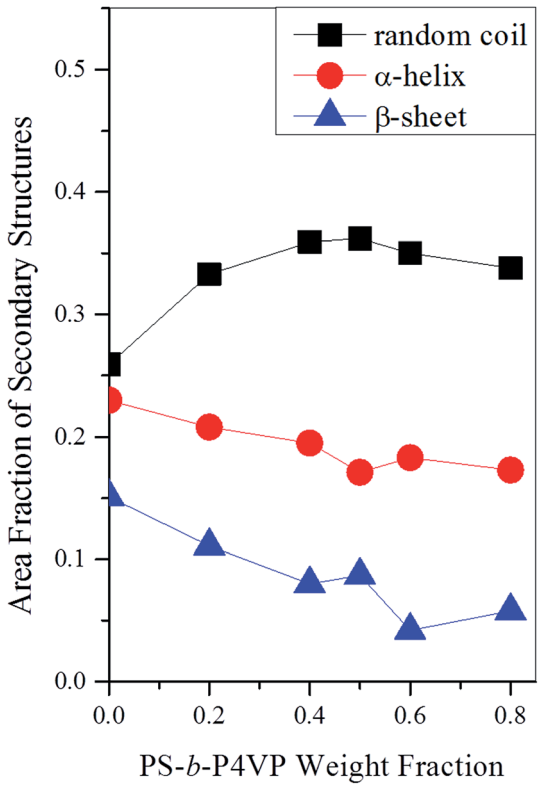

Fig. 3 Secondary structures in PS-*b*-P4VP/PTyr blend systems with various P4VP contents.

1683, and 1700 cm^{-1}.[13,32] Based on the results of curve fitting (Fig. 3 and S3†), the fractions of the α-helical and β-sheet conformations decreased, accompanied by an increase in the fraction of random coil conformations, with increasing PS-*b*-P4VP concentration, which is consistent with the wide angle X-ray diffraction (WAXD) patterns.

Fig. 4 displays the morphologies of the PS-*b*-P4VP/PTyr blend systems. The SAXS analysis of the pure PS-*b*-P4VP revealed the long-range order of a lamellar structure, based on peak positions in the ratio of 1 : 2 : 3 : 4 (Fig. 4a), as confirmed in the TEM images in Fig. 4b. After blending with PTyr at 20 wt%, the short-range order of a cylinder structure was evident through SAXS analysis (Fig. 4c), with a peak position ratio of 1 : $7^{1/2}$, as confirmed in the corresponding TEM image in Fig. 4d. When the weight percent of PTyr was 40–60%, the SAXS patterns featured a single broad peak, with the corresponding TEM images revealing spherical micelle structures (Fig. 4e–j). Thus, the morphological change observed upon increasing the concentration of PTyr in the PS-*b*-P4VP/PTyr blend system was from lamellae to cylinders and, finally, to spherical micelles. When the flexible polymer (PVPh)[31] and inorganic nanoparticles of (octakis[dimethyl(4-hydroxyphenethyl)siloxy] silsesquioxane (OP-POSS))[20] were blended with the PS-*b*-P4VP systems, the phenolic hydroxyl groups of both PVPh and OP-POSS formed hydrogen bonds with the P4VP blocks and resulted in an ordered morphological transition upon increasing the PVPh or OP-POSS concentrations. In contrast, blending with PTyr resulted in limited morphological transformations because of the rigid-rod characteristic of PTyr and the lower entropic change induced by the polypeptide chain.

To extend the applications of this system, we added the crosslinking agent (HMTA) into the PTyr matrix to improve the mechanical properties of the blend materials. Simply heating the system allowed crosslinking of the phenolic groups of PTyr. After such heat-treatment, the physical properties improved, especially the thermal properties. In addition, the crosslinked systems could not be re-dissolved in DMF because of the high degree of crosslinking. DSC revealed (Fig. S4a†) that the value of T_g increased substantially in the P4VP/PTyr complex phase (by approximately 10–35 °C). In addition, the glass transition temperature behavior could also be fitted to the Kwei equation, as displayed in Fig. S4b;† we obtained values of k and q of 1 and 250, respectively, with the latter significantly higher than for the PS-*b*-P4VP/PTyr blend system without crosslinking (q = 135). This behavior presumably arose because of the formation of crosslinking points, which further restricted the mobility of the polymer chains and thus increased the value of T_g. Similarly TGA analysis revealed higher residues or char yields from the crosslinked samples after heating to 800 °C, compared with those of the non-crosslinked sample (Fig. S5a and b†). Thus, both DSC and TGA analyses confirmed that the crosslinked PTyr materials possessed thermal properties superior to those of the non-crosslinked samples.

The XRD analysis of the crosslinked blend systems in Fig. S6a† reveals that the pure crosslinked PTyr retained the signal at 18°, representing the distance between lamellar layers. We conjecture that the crosslinking process in PTyr occurred mostly through the phenolic groups on the side-chains of the polypeptide. This peak disappeared when the concentration of PS-*b*-P4VP was greater than 40 wt%, with the XRD patterns

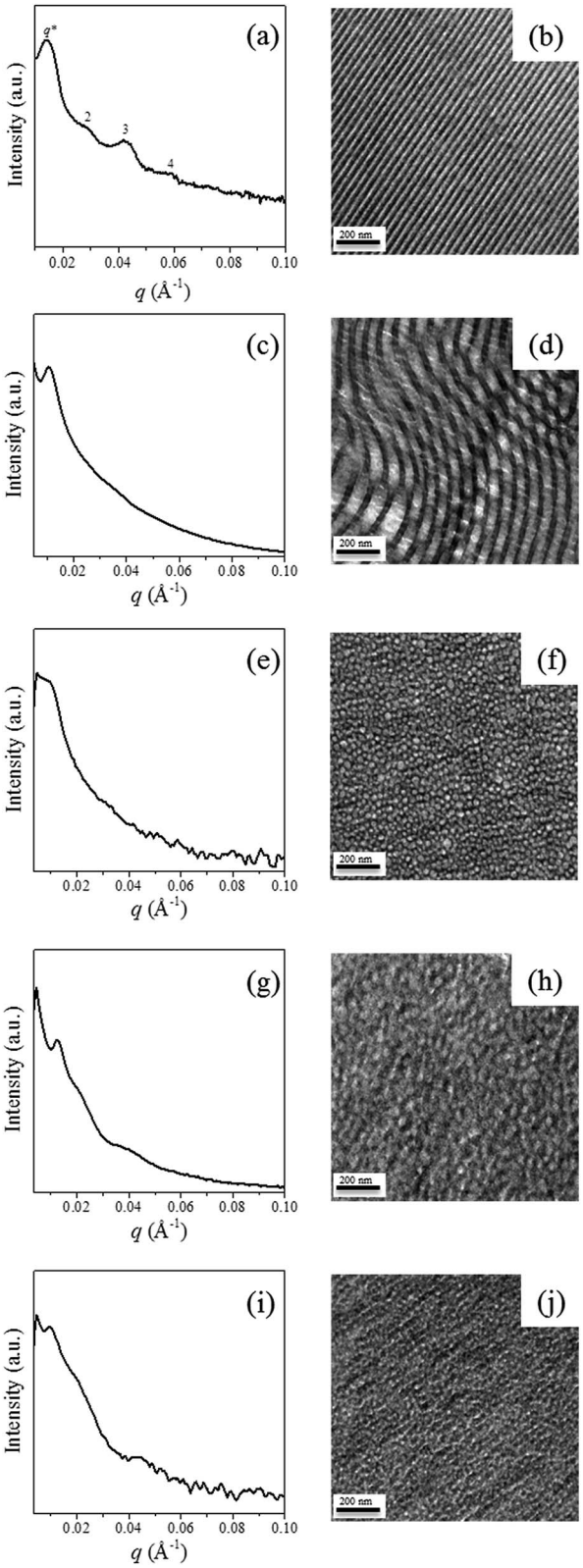

Fig. 4 (Left) SAXS patterns and (right) corresponding TEM images of PS-*b*-P4VP/PTyr blends in ratios of (a) and (b) 100/0, (c) and (d) 80/20, (e) and (f) 60/40, (g) and (h) 50/50, and (i) and (j) 40/60.

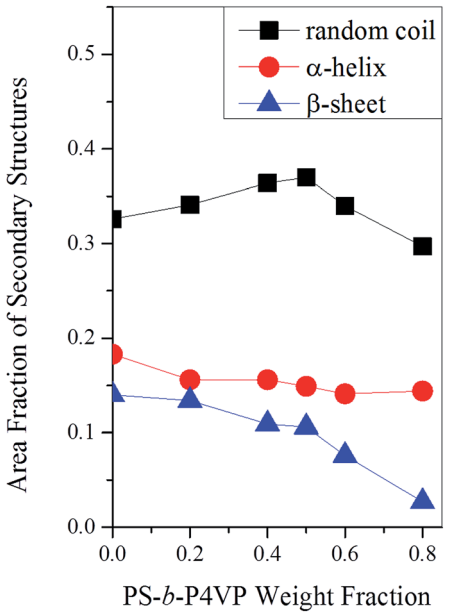

Fig. 5 Secondary structures in the crosslinked PS-*b*-P4VP/PTyr blend systems with various P4VP contents.

showing broad amorphous halos after thermal crosslinking. FT-IR spectroscopic analysis (Fig. S6b and S7†) also revealed the change in the secondary structure of the crosslinked PTyr; Fig. 5 summarizes the results from curve-fitting. Similar to the behavior of the non-crosslinked blend systems, the content of random coil conformations increased while those of the α-helix and β-sheet conformations decreased. Table S1† summarizes the proportions of the secondary structures before and after crosslinking of the blend systems. After crosslinking, there is a slight decrease in the contents of the α-helix, β-sheet, and random coil conformations, revealing that the crosslinking process did indeed influence the self-assembly of the PTyr secondary structures.

SAXS and TEM analysis revealed the morphologies of the crosslinked blend systems (Fig. 6). Again, the pure PS-*b*-P4VP revealed the long-range order of a lamellar structure (Fig. 6a and b). After blending with 20 wt% crosslinked PTyr, body-centered cubic (BCC) spherical structures were observed, based on the TEM image in Fig. 6d. Upon further increasing the PTyr concentration with HMTA, the *d*-spacings decreased, as determined from the first peaks by SAXS analysis at 0.01 $Å^{-1}$ (62.8 nm) in Fig. 6e, 0.011 $Å^{-1}$ (57.0 nm) in Fig. 6g and 0.013 $Å^{-1}$ (48.3 nm) in Fig. 6i. The morphology was not obviously different from that of the non-crosslinked sample, but it did display better uniformity because the crosslinking reaction could enhance the microphase separation by increasing the molecular weight of the polypeptides.

In mercury adsorption experiments, since Hg(II) ions tend to form $Hg(OH)_2$ and precipitate from aqueous solution, an acidic solution (pH ≈ 2.85) can be chosen to avoid this precipitation and simplify the observation process. To calculate the mercury loading, the adsorption capacity (mg g^{-1}) at equilibrium was obtained as follows:

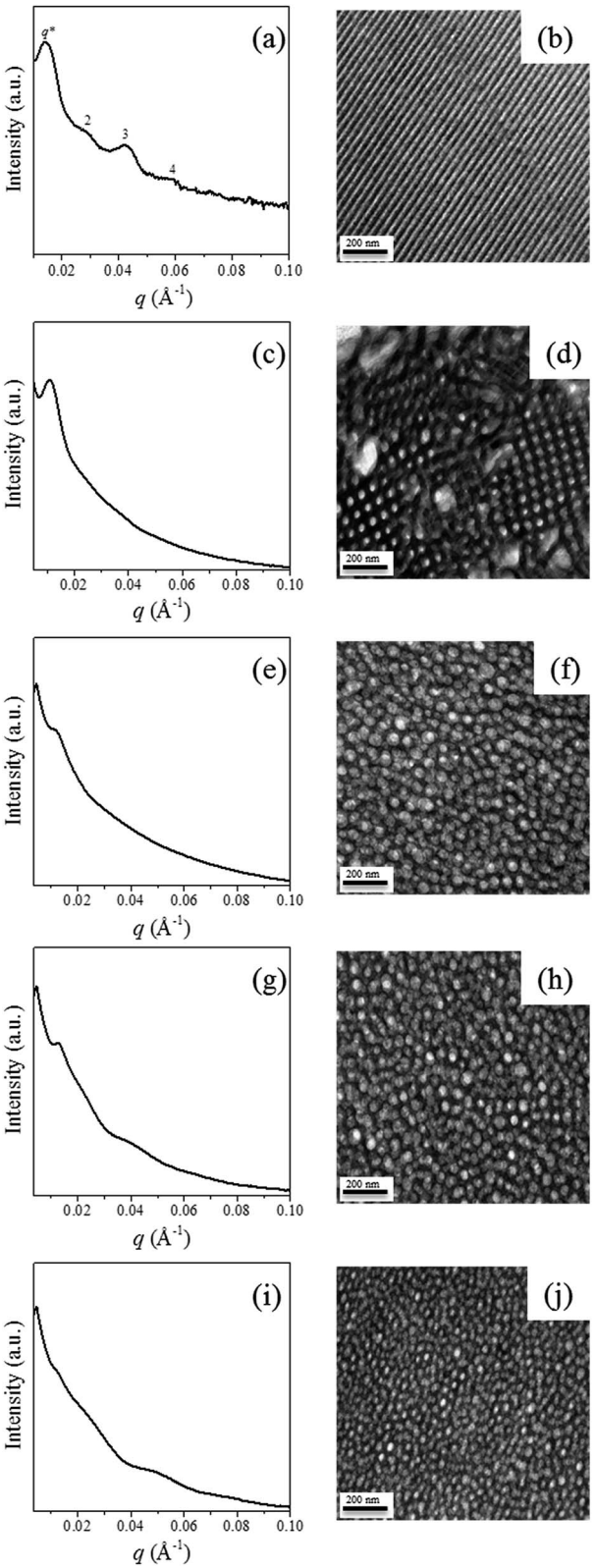

Fig. 6 (Left) SAXS patterns and (right) corresponding TEM images of crosslinked PS-*b*-P4VP/PTyr blends in ratios of (a) and (b) 100/0, (c) and (d) 80/20, (e) and (f) 60/40, (g) and (h) 50/50, and (i) and (j) 40/60.

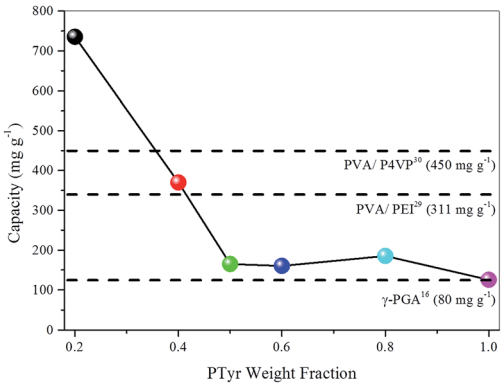

Fig. 7 Mercury(II) adsorption capacities (mg g^{-1}) calculated from ICP-OES data.

$$\text{Capacity} = \frac{(C_0 - C_{eq})V}{m_D} \quad (2)$$

where C_0 and C_{eq} (mg L^{-1}) are the initial and equilibrium concentrations of the Hg(II) solution, respectively; V (L) is the volume of the solution; and m_D (g) is the mass of a variety of crosslinked samples with different ratios. We calculated the value of the capacity of each crosslinked sample from ICP-OES (Fig. 7). The pure crosslinked PTyr had a mercury capacity of 125 mg g^{-1}; its adsorption ability was better than that of γ-PGA, as determined in a previous study.[16] The stability arising from the crosslinking process may have been responsible for raising the efficiency. Furthermore, FT-IR spectra revealed that the peak at 2945 cm^{-1}, representing N–H stretching, disappeared after the adsorption of mercury, which is evidence that PTyr combines with mercury through its amido groups.[16] Upon the addition of PS-*b*-P4VP, the signal in the FT-IR spectrum for the free pyridyl rings at 993 cm^{-1} disappeared completely, regardless of the amount of P4VP. We suspect that the mercury ions were bound to the pyridyl rings through ionic dipole interactions.[30] The highest value of capacity (735.5 mg g^{-1}) was that obtained in the presence of 20 wt% PTyr, presumably because this ratio provided the highest content of free pyridyl rings (Fig. 2b), as well as the long-range-ordered self-assembled structure displayed in Fig. 6d. Because both the matrix and the template could adsorb mercury ions, the crosslinked PS-*b*-P4VP/PTyr displayed very high capacity for mercury adsorption relative to those of PVA/PEI (311 mg g^{-1})[29] and PVA/P4VP (450 mg g^{-1}),[30] thereby improving the efficiency of mercury ion adsorption. At the same time, the bio-characteristics of PTyr suggest that it will be eco-friendly.

Conclusions

The morphologies of PS-*b*-P4VP/PTyr blend systems are influenced by hydrogen bonding interactions between the P4VP block and the PTyr. This system provides an alternative means of controlling the polypeptide's self-assembly in the bulk state. Crosslinking of the PTyr side chains provides a means of

improving the system's thermal properties and stabilizing its structures. Because they can bind to the pyridyl rings of P4VP and the amido groups of PTyr, mercury ions adsorbed strongly to the crosslinked PS-*b*-P4VP/PTyr. This approach should improve the removal of mercury in wastewater quality indicators. Furthermore, with the active functional groups, biocompatibility and mechanical stability characteristics of crosslinked PTyr, it can be applied in biological experiments in future works.

Acknowledgements

This study was supported financially by the Ministry of Science and Technology, Republic of China, under contracts MOST 103-2221-E-110-079-MY3 and MOST 105-2221-E-110-092-MY3. Dr Yi-Chen Wu also thanks 2014 New Partnership Program for the Connection to the Top Labs in the World under contracts MOST 104-2911-I-110-503 that helped initiate this study. The authors extend their appreciation to the International Scientific Partnership Program (ISPP) at King Saud University (KSU) for funding this research work through ISPP-0024.

References

1 P. B. Malafaya, G. A. Silva and R. L. Reis, *Adv. Drug Delivery Rev.*, 2007, **59**, 207–233.
2 T. J. Deming, *Adv. Mater.*, 1997, **9**, 299–311.
3 Y. F. Huang, S. C. Lu, Y. C. Huang and J. S. Jan, *Small*, 2014, **10**, 1939–1944.
4 Y. Li, B. P. Bastakoti, M. Imura, S. M. Hwang, Z. Sun, J. H. Kim, S. X. Dou and Y. Yamauchi, *Chem.–Eur. J.*, 2014, **20**, 6027–6032.
5 Y. Li, B. P. Bastakoti and Y. Yamauchi, *Chem.–Eur. J.*, 2015, **21**, 8038–8042.
6 D. E. Meyer and A. Chilkoti, *Biomacromolecules*, 2002, **3**, 357–367.
7 S. Zhang, *Nat. Biotechnol.*, 2003, **21**, 1171–1178.
8 H. A. Klok and S. Lecommandoux, *Adv. Mater.*, 2001, **13**, 1217–1229.
9 P. Papadopoulous, G. Floudas, H. A. Klok, I. Schnell and T. Pakula, *Biomacromolecules*, 2004, **5**, 81–91.
10 C. T. Pan, C. K. Yen, H. C. Wu, L. Lin, Y. S. Lu, J. C. C. Huang and S. W. Kuo, *J. Mater. Chem. A*, 2015, **3**, 6835–6843.
11 S. W. Kuo and C. J. Chen, *Macromolecules*, 2011, **44**, 7315–7326.
12 S. W. Kuo and C. J. Chen, *Macromolecules*, 2012, **45**, 2442–2452.
13 Y. S. Lu, Y. C. Lin and S. W. Kuo, *Macromolecules*, 2012, **45**, 6547–6556.
14 Y. S. Lu and S. W. Kuo, *RSC Adv.*, 2015, **5**, 88539–88547.
15 H. Liu and H. H. P. Fang, *Biotechnol. Bioeng.*, 2002, **80**, 806–811.
16 B. S. Inbaraj, J. S. Wang, J. F. Lu, F. Y. Siao and B. H. Chen, *Bioresour. Technol.*, 2009, **100**, 200–207.
17 J. Sun, C. Deng, X. Chen, H. Yu, H. Tian, J. Sun and X. Jing, *Biomacromolecules*, 2007, **8**, 1013–1017.
18 A. Rahikkala, S. Junnila, V. Vartiainen, J. Ruokolainen, O. Ikkala, E. Kauppinen and J. Raula, *Biomacromolecules*, 2014, **15**, 2607–2615.
19 C. Liang, K. Hong, G. A. Guiochon, J. W. Mays and S. Dai, *Angew. Chem., Int. Ed.*, 2004, **43**, 5785–5789.
20 R. Saito, *Macromolecules*, 2001, **34**, 4299–4301.
21 Y. S. Lu, C. Y. Yu, Y. C. Lin and S. W. Kuo, *Soft Matter*, 2016, **12**, 2288–2300.
22 Y. S. Lu and S. W. Kuo, *RSC Adv.*, 2014, **4**, 34849–34859.
23 C. J. Clarke, A. Eisenberg, J. La Scala, M. H. Rafailovich, J. Sokolov, Z. Li, S. Qu, D. Nguyen, S. A. Schwarz, Y. Strzhemechny and B. B. Sauer, *Macromolecules*, 1997, **30**, 4184–4188.
24 W. van Zoelen, G. Alberda ten, O. Ikkala and G. ten Brinke, *Macromolecules*, 2006, **39**, 6574–6579.
25 G. Alberda ten, R. Meyboom, G. ten Brinke and O. Ikkala, *Macromolecules*, 2000, **33**, 3752–3756.
26 R. S. Vieira and M. M. Beppu, *Water Res.*, 2006, **40**, 1726–1734.
27 J. M. Pacyna and J. Munch, *Water, Air, Soil Pollut.*, 1991, **56**, 51–61.
28 R. K. Zalups, *Pharmacol. Rev.*, 2000, **52**, 113–144.
29 H. Bessbousse, T. Rhlalou, J. F. Verchère and L. Lebrun, *J. Membr. Sci.*, 2008, **325**, 997–1006.
30 H. Bessbousse, T. Rhlalou, J. F. Verchère and L. Lebrun, *J. Phys. Chem. B*, 2009, **113**, 8588–8598.
31 J. Wang, M. K. Cheung and Y. Mi, *Polymer*, 2001, **42**, 3087–3093.
32 Y. E. Khoury, R. Hielscher, M. Voicescu, J. Gross and P. Hellwig, *Vib. Spectrosc.*, 2011, **55**, 258–266.

